NANO LETTERS

Letter

pubs.acs.org/NanoLett

Atomic Layer Deposition from Dissolved Precursors

Yanlin Wu,[†] Dirk Döhler,[†] Maïssa Barr,[¥] Elina Oks,[‡] Marc Wolf,[‡] Lionel Santinacci,[¥] and Julien Bachmann*[,†,‡]

[†]Department of Chemistry and Pharmacy, Friedrich-Alexander University of Erlangen-Nürnberg, Egerlandstrasse 1, D−91058 Erlangen, Germany

[¥]CNRS, CINaM UMR 7325, Aix Marseille Université, F−13288 Marseille, France

[‡]Departments of Chemistry and Physics, University of Hamburg, Sedanstrasse 19, D−20146 Hamburg, Germany

Supporting Information

ABSTRACT: We establish a novel thin film deposition technique by transferring the principles of atomic layer deposition (ALD) known with gaseous precursors toward precursors dissolved in a liquid. An established ALD reaction behaves similarly when performed from solutions. "Solution ALD" (sALD) can coat deep pores in a conformal manner. sALD offers novel opportunities by overcoming the need for volatile and thermally robust precursors. We establish a MgO sALD procedure based on the hydrolysis of a Grignard reagent.

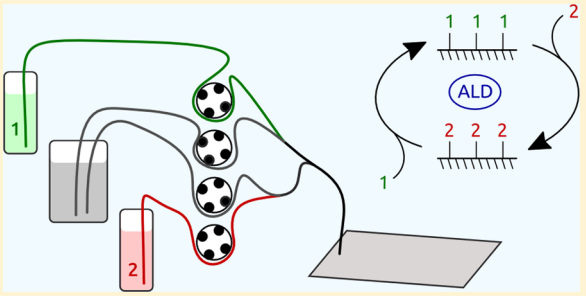

KEYWORDS: *Atomic layer deposition, LBL, SILAR, thin films, magnesium oxide, microfluidic*

Atomic layer deposition, or ALD, is a thin film deposition technique based on self-limiting surface chemistry.[1,2] In ALD, the solid surface is exposed in alternating manner to two (or more) gaseous reagents, or precursors, each of which adsorbs irreversibly by reacting with the chemically reactive groups on the surface. Because at each step the reaction stops after all available surface groups have been occupied, the amount of material deposited is not limited by the dosage of precursors. Instead, each pair of consecutive reactions results in the deposition of a well-defined solid thickness and can be repeated in a cyclic manner. Overall, the film thickness only depends on the number of ALD cycles performed. One outstanding consequence of this self-limiting property is the capability of the technique to coat nonplanar substrates, in particular highly porous ones.[3−7]

To date, ALD has been applied successfully to the deposition of fluorescent materials in displays, high-κ dielectrics, passivating layers in solar cells, as well as many other noncommercial device layers. A large fraction of the periodic table can be deposited as oxides by ALD, whereas some sulfides, nitrides, selenides, and elemental noble metals are also known ALD materials.[1] Organic building blocks have been used in ALD-like depositions to generate "molecular layer deposition" or MLD, albeit with limited generality. Currently, the range of ALD-grown materials is limited by the availability of ALD precursors: in particular, precursors not only need to be highly reactive and specific, but also they have to generate sufficient vapor pressure below their decomposition temperature. Indeed, ALD has always been considered a deposition method from the gas phase exclusively. This is due in part to historical reasons, given that early ALD scientists originated from the CVD (chemical vapor deposition) and MBE (molecular beam epitaxy) communities.[8,9]

We now propose to complement this ALD from the gas phase, or gALD, with ALD from liquid solutions of precursors, or sALD.

Indeed, the characteristics of ALD as described earlier (complementary, self-limiting surface reactions) are not explicitly limited to gaseous reagents. Therefore, we contend that these reaction principles can be transferred to the dissolved phase. In fact, some surface treatment methods exist that base on related ideas. The "layer-by-layer" (LBL) growth of polymer films uses alternating exposures of the substrate to two solutions of oppositely charged polyelectrolytes.[10−12] At each step, the amount deposited is approximately defined by a local electrostatic balance. In a completely different field of research, "quantum dot" nanocrystals (typically of the II−VI semiconductors) have been overcoated with a wide-bandgap layer by "successive ionic layer adsorption and reaction" (SILAR), whereby the quantum dot suspension is exposed to alternating solutions of two salts resulting in a shell of the desired binary compound, if the driving force for its formation is sufficient.[13,14] In practice, SILAR has been limited to a few cycles only. Finally, electrochemical ALD has long been known and exploits underpotential deposition of two elements in alternating, repeating manner.[15,16] The method is limited in terms of materials achievable and the thickness to be reached via repeated electrolyte changes.

Received: April 13, 2015
Revised: September 23, 2015
Published: September 29, 2015

DOI: 10.1021/acs.nanolett.5b01424
Nano Lett. 2015, 15, 6379−6385

These three methods confirm that the "self-limiting" growth of binary compounds is possible from dissolved precursors as well as in gALD, but they lack generality and practicality. In the current paper, we introduce solution ALD (sALD) as a method as general and practical as gALD: (1) we develop a setup for sALD and find appropriate experimental parameters; (2) we demonstrate the similarity of sALD with gALD for a known reaction; (3) we develop an sALD reaction that is impossible to perform in regular ALD; and (4) we characterize an sALD deposition in deep pores.

In regular ALD, gaseous precursors are brought into the reaction chamber (which contains the substrate under vacuum conditions) via a set of computer-controlled valves. Handling liquids instead of gases is possible with much simpler, less expensive equipment available in any chemical synthesis laboratory, namely Schlenk glassware. The dosage of precursors, which are defined in gALD by the temperature of the precursor bottles and the duration of the valve opening, can be set in sALD with solution concentration and liquid volumes determined by pumps such as syringe pumps or peristaltic pumps. We choose the latter for cost reasons and for their capability of handling unlimited amounts of liquid. The vision presented in Figure 1 is that four peristaltic pumps connected

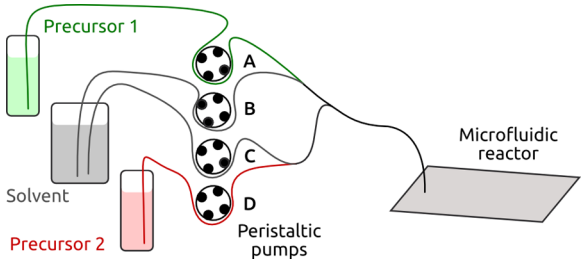

Figure 1. Principle view of the sALD setup. Four peristaltic pumps (labeled A through D) deliver the precursors and solvent to the microfluidic reaction chamber in alternating manner. The delivery of solvent into the lines A and D prevents the direct contact between both precursors.

to both precursor solutions and a pure solvent container deliver the liquids in alternating manner into a microfluidic chamber containing the substrate to be coated. The pulse and pump times defined in gALD are replaced by durations of pump A or D function (precursor 1 or 2 pulse) and of pump B and C function (solvent purge), respectively.[17]

Both precursors and solvent are brought into a single tube delivering the liquid to the reaction chamber. The geometry of the tube system is designed in a way such that both precursor solutions cannot come in contact with each other. This is the reason for the presence of two solvent lines flushing a segment of tube from precursor 1 and precursor 2 after each pulse. We note that the geometry of the tubes affects the results of the sALD procedures or that it must be accounted for when defining the other experimental parameters. Indeed, long segments of tube make it necessary to increase the durations of pulses and purges, whereas very short segments may bear the risk of back-diffusion of precursors, if the liquid were to stay immobile for long times.

We designed two distinct chambers for planar and porous substrates (Figure 2). In the former case, the precursor solutions are flown over the sample, and in the latter, they are forced to flow through the pores. The planar chamber consists of a milled Teflon plate defining a recessed area (gray color in

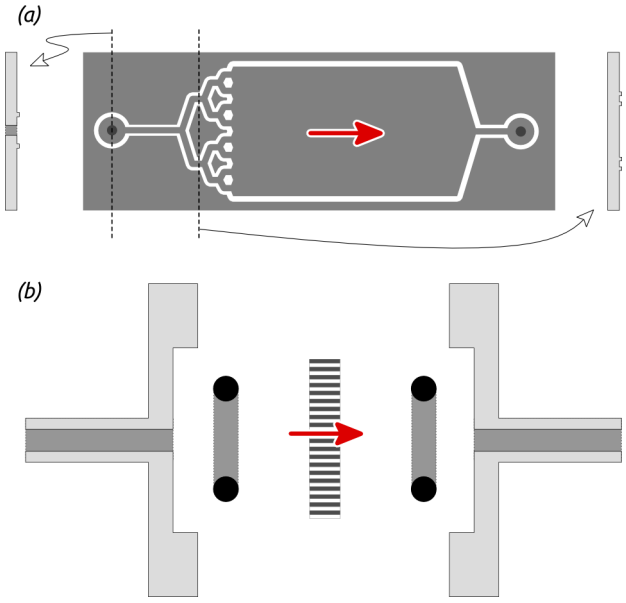

Figure 2. Schemes of sALD sample chambers. (a) Teflon chamber based on "flow-by" of a planar sample. A top view is presented in the center along with two cross-sections. The total length of the Teflon plate is 7.6 cm, whereas the height and thickness of the walls are 1 mm. (b) Stainless steel chamber for "flow-through" of nanoporous samples (sketched in the center with pores not on scale), presented in cross-section. The red arrow represents the direction of liquid flow.

Figure 2a) surrounded by walls of 1 mm height. The sample (a fragment of Si wafer) is placed in the recess, and the chamber is closed by a microscope slide clamped onto the Teflon plate. The liquids are brought by the tube system into the sample chamber via a bore hole at one extremity, they then flow toward the other extremity (from left to right on Figure 2a), and they finally exit the chamber via another bore hole. A branched geometry of channels near the chamber entrance allows for a most uniform, laminar flow across the chamber. Nanoporous samples could not be coated conformally in this "flow-by" chamber due to the slow diffusion into deep pores. Therefore, we opt for a "flow-though" design in which the sample sealed by two O-rings is clamped between two plates carrying the tube connections (Figure 2b). Care must be taken to minimize the volume of liquid contained between plate and sample since it does not support laminar flow and therefore causes undesired mixing. To prevent excessive pressure upstream of the nanoporous structure, the speed of the peristaltic pumps must be reduced. The pulse and purge durations are increased correspondingly so that the total liquid volumes are maintained.

The first benchmark of our sALD method and setup will be a well-established ALD reaction. We will first demonstrate the self-limiting behavior characteristic of ALD and compare the growth rate with that known for the gas-phase process.

We focus on the hydrolysis of titanium(IV) isopropoxide, $Ti(^{i}OPr)_4$, a reaction that has been used in the gas phase between room temperature and approximately 200 °C.[18−20] By using diethyl ether solutions and the standard parameters listed in Table S1 in the Supporting Information, a series of samples (Si wafers with thermal oxide layer) treated with increasing numbers of TiO_2 sALD cycles at room temperature deliver a growth line presented in Figure 4, panel a. The least-squares regression line cuts the origin within uncertainty ($R^2 > 0.99$), indicating the absence of nucleation inhibition. The growth rate

DOI: 10.1021/acs.nanolett.5b01424
Nano Lett. 2015, 15, 6379−6385

is 0.3 Å per cycle, well within the (rather broad) range of TiO_2 gALD growth rates reported in literature precedents.[18−20] The films are amorphous and have a somewhat higher roughness than their gALD counterparts, as shown by transmission electron micrographs (TEM) of thin sample slices (Figure 3).

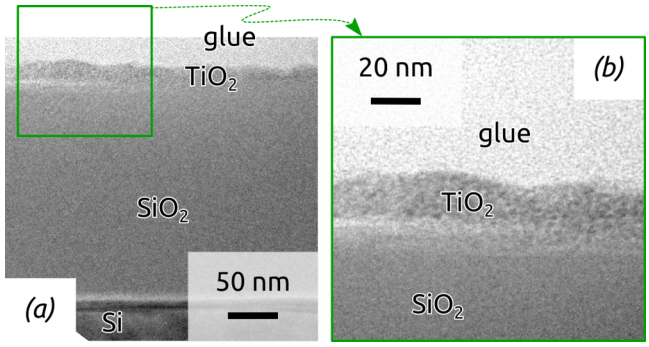

Figure 3. Transmission electron micrographs of a thin TiO_2 film grown by sALD on a Si wafer with 200 nm of thermal SiO_2. The identity of the individual phases observed is labeled. The region framed in panel a is presented at a higher magnification in panel b.

Crucial for the definition of ALD chemistry is the characterization of growth rate as it depends on precursor dosage. An ALD cycle must consist of individual surface reactions that stop on their own after having covered the full surface with an adlayer. Thus, beyond a certain minimal precursor dosage necessary for reaching full monolayer coverage, the deposition rate must be independent of dosage. This has been the gold standard of novel gALD reactions to date.[21,22] This property is found in our TiO_2 sALD reaction as well. Figure 4, panel b demonstrates that, all other parameters being kept equal to the values from Table S1, surface saturation by $Ti(^iOPr)_4$ is achieved at approximately t_1 = 10 s. Shorter pulses deliver too little $Ti(^iOPr)_4$ for full coverage, and excess $Ti(^iOPr)_4$ does not increase the amount deposited at each cycle.

The chemical identity of the films is characterized by X-ray photoelectron spectroscopy (XPS, Figure 5). The O 1s region (Figure 5a) contains exactly two components, associated with TiO_2 and the wafer's thermal SiO_2, at 530.0 and 532.3 eV, respectively. The Ti 2p region only consists of the $2p_{3/2}/2p_{1/2}$ doublet of stoichiometric TiO_2 at 464.3 and 458.6 eV,[23,24] also observed with gALD TiO_2 films.[23,24] Thus, the XPS data are consistent with pure TiO_2.

To demonstrate the advantage of our novel sALD method in terms of being able to use inexpensive and highly reactive but nonvolatile precursors, we now turn to magnesium oxide. This interesting dielectric is typically deposited by gALD from bis(ethylcyclopentadienyl)magnesium (or the parent Cp_2Mg) and dioxygen (or ozone or water).[25,26] Grignard reagents, RMgX (with R an alkyl group and X a halide), have long been established in organometallic chemistry as highly hydrolytically reactive and cost-effective reagents. In fact, the molar price of EtMgCl is about 1/100 that of $(EtCp)_2Mg$. However, the aggregation behavior of Grignard reagents makes them impossible to use in gALD. They do not exist as isolated, unsolvated molecules and decompose before vaporizing.

Our novel MgO sALD reaction displays particularly well-behaved and advantageous characteristics. The ellipsometry data (Figure 6) evidence that the film obtained from EtMgCl + H_2O by sALD consists of pure MgO. We note that all

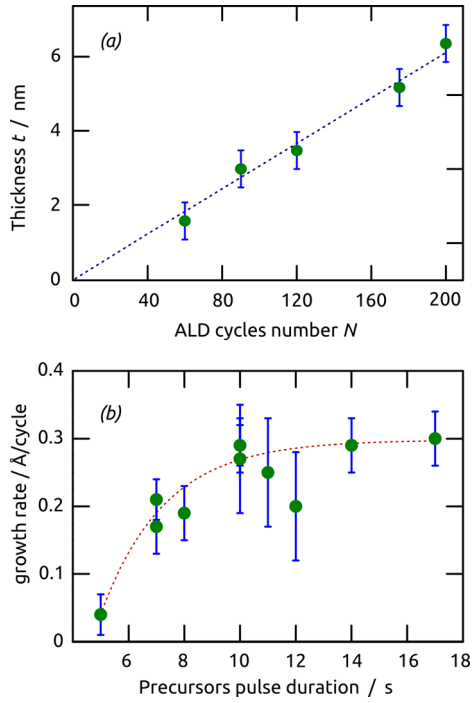

Figure 4. Typical ALD characteristics of a gALD process transferred into sALD: the hydrolysis of $Ti(^iOPr)_4$ to TiO_2. (a) The solid film thickness (measured by spectroscopic ellipsometry on a silicon wafer with 200 nm thermal oxide) increases in direct proportionality to the number of sALD cycles performed. The blue dotted curve is a least-squares linear fit. (b) The growth rate (quantified as growth per cycle) saturates at a certain precursor dosage, after which it remains constant, reflecting the self-limiting characteristic of the sALD process. Note that the pulse durations are kept identical for $Ti(^iOPr)_4$ and H_2O so that a simultaneous variation of the dosage of both precursors is presented. The experimental uncertainty of ±0.5 nm on spectroscopic ellipsometry measurements is indicated by blue error bars. The red dotted line is a least-squares exponential fit.

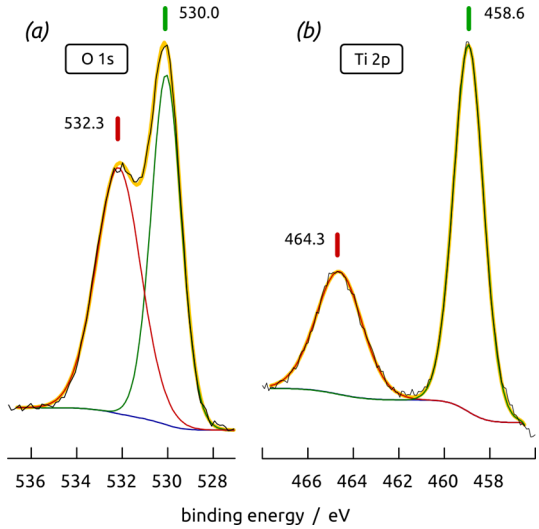

Figure 5. XPS of an sALD TiO_2 film on an Si/SiO_2 substrate: (a) O 1s region, (b) Ti 2p region. Black, experimental data points; blue, background; red and green, individual components; yellow, fit curve. The energies of the peaks are given on the graphs.

conceivable byproducts of the reactions (EtH, EtOH, and HCl) are soluble in Et_2O at the concentrations relevant here, as

DOI: 10.1021/acs.nanolett.5b01424
Nano Lett. 2015, 15, 6379−6385

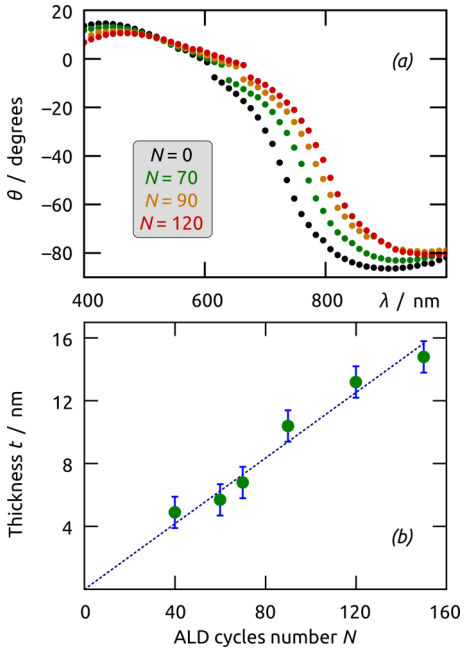

Figure 6. Characteristics of MgO sALD from EtMgCl + H_2O (at room temperature in Et_2O). (a) Spectroscopic ellipsometry traces (orientation $\theta(\lambda)$) of one Si/SiO_2 wafer submitted to increasing numbers N of sALD cycles, evidencing the systematic film thickness increase. (b) Growth curve determined from the ellipsometry data, evidencing the linear behavior with 1 Å per cycle growth rate. The experimental uncertainty on film thickness is ±1 nm.

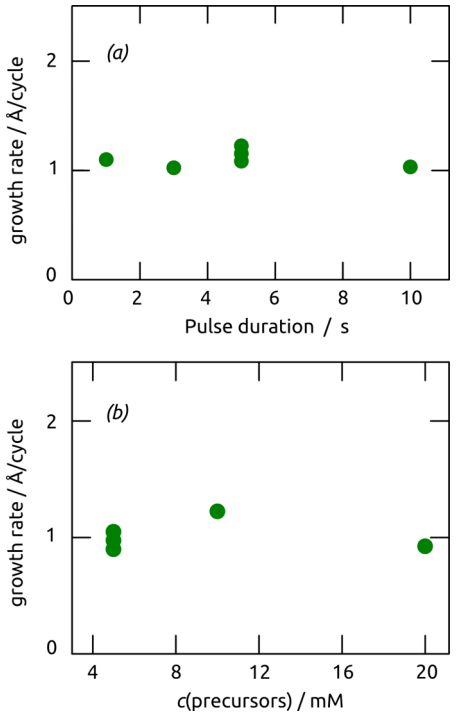

Figure 7. Experimental dosage-growth behavior of the MgO sALD reaction EtMgCl + H_2O. The growth rate is independent of both the (a) precursor concentrations and (b) pulse durations, two distinct ways of varying the dosage. In this study, we have varied the concentrations of both precursors and both pulse durations simultaneously.

opposed to the solid MgO. The saturated growth is highly linear ($R^2 > 0.99$), presents no nucleation inhibition, and occurs at a high rate of 1 Å per cycle. This growth rate, albeit high, is similar to the values previously reported in gALD processes.[25,26] It also can be expected based on the small size of the ligands on the inorganic center.

The self-limiting (ALD) behavior of the reaction is demonstrated by the graphs determining the influence of the precursors' concentration and the pulse duration on the deposition rate, Figure 7. The concentrations of EtMgCl and water can be varied between 5 mM and 20 mM, and the pulse durations between 1 and 10 s, without any change in the growth rate. Thus, the reaction is highly robust in our set of experimental conditions.

One unique capability of ALD, which is directly related to its self-limiting surface chemistry, is its capability to coat deep pores in a conformal manner.[3−7] This is also of particular importance for applications based on interfaces of large geometric area.[27] For example, we have recently exploited gALD-grown silica layers toward negative lithium ion battery electrode materials after thermal reduction to elemental Si.[28] In gALD, we had circumvented the relative inertness of the Si−O bond by a three-step reaction scheme involving an aminoalkyl-functionalized silicon precursor, water, and ozone.[29] However, the use of halide precursors, which is hazardous in gALD due to the corrosive nature of HCl gas, can simplify ALD chemistry in the sALD concept. Thus, we use $HSiCl_3$ and water as the precursors for silica sALD, and we will apply the reaction to "anodic" nanoporous oxide substrates. The substrates were made in-house and feature pores of approximately 300 nm diameter and 30 μm length.

First of all, the growth rate of the $HSiCl_3$ + H_2O reaction was determined by ellipsometry on a planar Si wafer (Figure 8a) to approximately 1.7 Å per cycle. This quite large value is comparable to cases reported using $SiCl_4$ + H_2O in gALD.[30,31] Further, we demonstrate the self-limiting property of the reaction (growth rate independence on precursor dosage) in nanoporous samples. The silica amount was quantified near the center of the 30-μm thick membrane by energy-dispersive X-ray spectroscopy (EDX) in a scanning electron microscope (SEM) as the intensity ratio between the Si and Al peaks (whereby the Al signal stemming from the matrix serves as internal standard). Figure 8, panel b, reports this ratio, normalized to the number of sALD cycles performed (f_{SiAl}), for three distinct concentrations of trichlorosilane and water. We observe the same saturating behavior as on planar samples, albeit at larger concentrations. This is logical given the significantly larger surface area to be coated.

The morphology of the deposit is observed in SEM, Figure 9, panels a and b. A top view of a nanoporous alumina membrane after sALD treatment is presented in Figure 9, panel a, and demonstrates a very clean sample. This proves that no silica is obtained via uncontrolled direct reaction between dissolved precursors (such direct reaction, considered "chemical vapor deposition" (CVD) in gas-phase conditions, would generate large particles retained on top of the pores in a sort of filtration effect). In higher magnification (inset), small particles of a few tens of nanometers appear on the inner pore walls. Such particles certainly do not correspond to the typical schematic presentation of ALD, in which perfect monolayers added sequentially result in a smooth, continuous film.[1] However, gALD often also yields particles as a consequence of hindered nucleation.[1,32−35] In that respect, the results obtained here with sALD are not different from those of gALD.

DOI: 10.1021/acs.nanolett.5b01424
Nano Lett. 2015, 15, 6379−6385

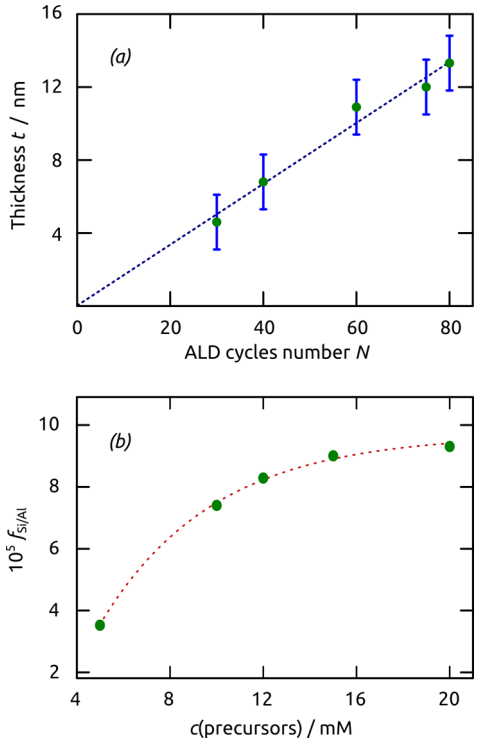

Figure 8. Characteristics of the sALD silica reaction from $HSiCl_3$ and H_2O. (a) Growth rate (1.7 Å per cycle) determined by spectroscopic ellipsometry on planar Si wafer pieces. The dotted blue line is a least-squares linear fit. (b) Self-limiting surface chemistry behavior observed in the middle of "anodic" nanoporous samples as a function of precursor dosage. The parameter f_{SiAl} quantifying the growth rate is defined in the text. The dotted red line is a least-squares exponential fit.

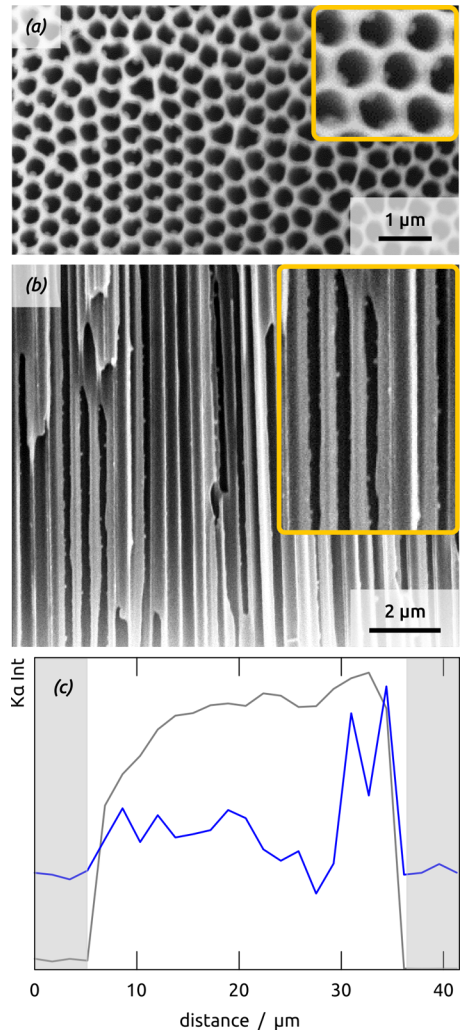

Figure 9. SEM investigation of nanoporous "anodic" samples coated with silica sALD. (a) Top SEM view showing that pores are not clogged; the more highly magnified inset reveals small silica particles. (b) Cross-section in which the pores appear homogeneously coated. (c) X-ray dispersive element profile of Si (blue) and Al (gray) along the pore length. Data points taken outside the sample are presented on a gray background.

The ALD material can be observed all along the pore length in cross-section (Figure 9b): they generate a certain roughness, which is absent in SEM observations of untreated pores. A further demonstration of the deposit's homogeneity along the depth axis is provided by EDX profiles. Figure 9, panel c displays the integrated EDX signals at the Al and Si Kα edges on an arbitrary scale (the Si signal was magnified to become comparable with that of Al). The Si signal, albeit weak and noisy, is nonzero over the full pore length and follows the curve for Al, which can be considered as an internal standard. The large signal near the right-hand pore extremity is a measurement artifact due to sample edge effects.

Thus, our sALD method is capable of coating deep pores (aspect ratio 100:1) with a thin layer of conformal thickness. This feature is not only interesting for applications, but also it is a further experimental demonstration of the self-limiting behavior (ALD nature) of the coating technique. Deviations from the perfect self-limiting surface chemistry result in a thickness decrease from top to bottom of the pores, and often to a thick continuous layer of deposit on top of the pore openings.

No undesired remnants of chlorides in the deposited solid can be observed by X-ray spectroscopy (Figure 10a). Only the expected elements Si, O, and Al appear (in addition to P from phosphoric acid anodization, C from surface contamination, and Cu and Ag from the sample holder). We attribute the Na signal to residual traces of salts in the solvent dried over the metal. In the as-prepared sample, the infrared spectrum (Figure 10b, top curve) is dominated by the prominent double peak of the asymmetric SiOSi stretch (TO and LO modes) in the region 1100−1200 cm^{-1},[36] together with the OH stretch region with adsorbed water near 3400 cm^{-1} and silanol near 3250 cm^{-1}.[35,37] A peak near 2250 cm^{-1} corresponds to a Si-bonded hydride stretch and hints at a substoichiometric silica.[38] However, adjusting the redox state of the material can be performed by annealing. After 4 h at 400 °C in aerobic atmosphere (Figure 10b, lower curve), both the hydrides and the surface silanol groups have disappeared. We note that the presence of hydroxides and hydrides is not a peculiarity of silica sALD, but is a general feature of silica ALD. It has been demonstrated that the removal of hydrides from SiO_2 can only be achieved by performing gALD at elevated temperature (550 °C) and in oxidizing conditions (H_2O_2).[39] Thus, the need to anneal the film after deposition does not represent an additional disadvantage of sALD.

The XPS data of as-deposited sALD silica films (Figure 11) do not evidence the presence of significant amounts of silanol groups, as the O 1s region of a sALD silica film on sapphire (Figure 11a) only shows two contributions associated with

DOI: 10.1021/acs.nanolett.5b01424
Nano Lett. 2015, 15, 6379−6385

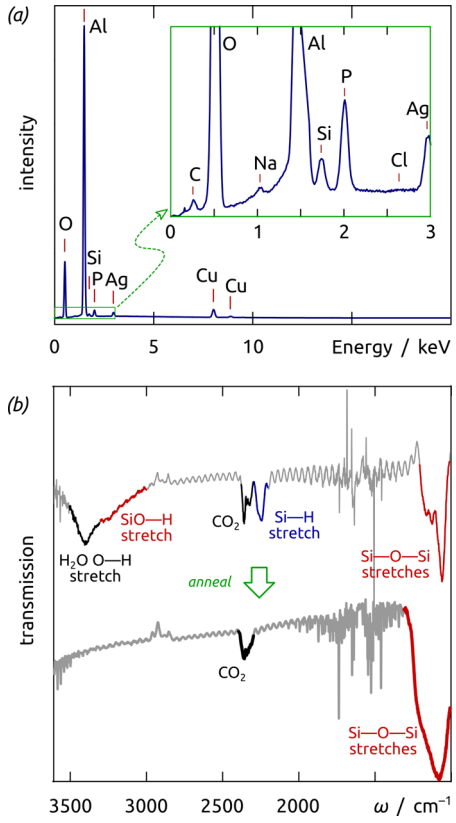

Figure 10. Chemical purity of the sALD silica material deposited on porous anodic alumina templates. (a) Energy-dispersive X-ray analysis (with scaled up section) showing the expected elements Si, O, and Al. P originates from the phosphate ions incorporated upon anodization in phosphoric acid, whereas Cu and Ag are due to the sample holder. The C signal from surface contamination is extremely small, and Cl is absent altogether. (b) Infrared difference spectra (with uncoated anodic template as the reference) of a silica-coated sample before (top thin curve) and after annealing at 400 °C in air (lower, thicker curve). Both spectra display the characteristic double peak of SiOSi stretches, whereas the Si–H and Si–OH initially present are removed upon annealing.

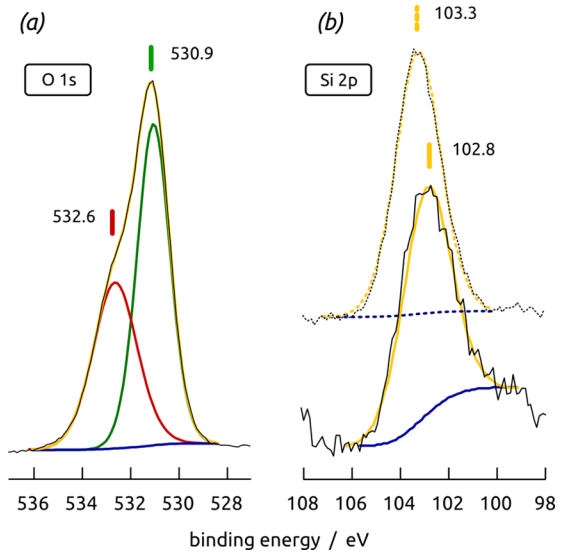

Figure 11. XPS spectra of silica sALD films on sapphire: (a) the O 1s region, (b) the Si 2p region. The as-deposited sample corresponds to the solid lines, whereas the dashed lines are obtained after annealing. Black, experimental data points; blue, background; red and green, individual components (if applicable); yellow, fit curve. The energies of the peaks are given on the graphs.

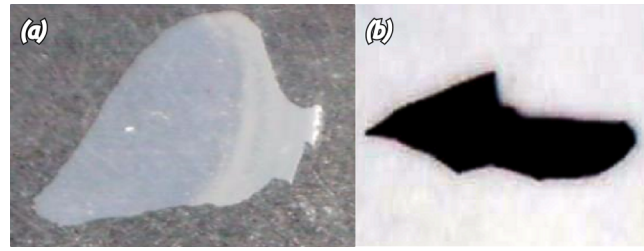

Figure 12. Photographs of a nanoporous "anodic" alumina sample (a) after coating by 60 cycles of silica sALD and (b) after subsequent thermal reduction of silica to amorphous Si with Li.

SiO_2 and Al_2O_3 at 532.6 and 530.9 eV, respectively.[40,41] The Si 2p region (Figure 11b) also displays a single peak after sALD at 102.8 eV. This peak, however, shifts to 103.3 eV upon annealing, which must be associated with the complete oxidation of the silica material also observed in IR spectroscopy (Figure 10).[40,41]

The macroscopic appearance of the samples also reveals successful sALD coating. Our nanoporous alumina substrates appear milky white due to light scattering by the 450 nm periodic structure. After coating with silica, the refractive index contrast between solid and pores is lower, which results in a more translucent appearance. The difference can be seen quite clearly in Figure 12, panel a, where a fragment of sample is pictured, the left-hand part of which has been coated, and the right-hand part has not been treated. The curvature of the O-ring sealing the sample is observable. Furthermore, subsequent thermal reduction of the silica coating with Li according to the published procedure causes the sample to turn to a lustrous black color (Figure 12b).[28] The sample color and its homogeneity are identical to those obtained by reduction of similar samples generated via silica gALD.[28]

Taken together, our results establish a novel thin film deposition technique. ALD, which to date had been known exclusively as a gas-phase technique, is now also applicable to liquid precursor solutions. The sALD method has similarities with previously existing surface treatment techniques such as LBL growth, SILAR, and electrochemical ALD, but it is much more general in terms of precursor (and corresponding thin film) chemical identities, substrate geometries, and film thicknesses. It is also practically easy to implement. First, the principles and chemical reactions valid in gALD are also applicable to sALD. The hydrolysis of titanium isopropoxide displays a similar growth rate in both experimental types of setups, and the self-limiting characteristic of the growth rate as a function of precursor dosage is common to both. Second, the novel sALD procedure can be utilized to coat deep pores conformally, similarly to what gALD is known for. Finally, and most importantly, sALD offers opportunities for novel types of ALD reactivity. The method overcomes the need for volatile and thermally robust precursors and opens the door to the broad diversity of reagents known in solution chemistry. Indeed, molecular inorganic and organic synthesis utilizes a number of highly reactive and highly specific reagents such as atom/group transfer agents, organometallics, as well as strong reductants, many of which only exist in aggregated phase.[42,43]

DOI: 10.1021/acs.nanolett.5b01424
Nano Lett. 2015, 15, 6379–6385

Thus, we expect that our novel sALD method will give access to materials that to date have been difficult or impossible to coat with traditional gALD.

■ ASSOCIATED CONTENT

Supporting Information

The Supporting Information is available free of charge on the ACS Publications website at DOI: 10.1021/acs.nanolett.5b01424.

Materials, instrumental methods, anodization of the nanoporous substrate, and sALD setup, Table S1 (PDF)

■ AUTHOR INFORMATION

Corresponding Author

*E-mail: julien.bachmann@fau.de.

Funding

This work was supported by the DFG Excellence Cluster 'Engineering of Advanced Materials' and by the European Research Council (ERC) under the European Union's Horizon 2020 research and innovation program (Grant Agreement No. 647281, 'Solacylin').

Notes

The authors declare no competing financial interest.

■ ACKNOWLEDGMENTS

We thank Prof. Martin Trebbin (University of Hamburg) for helpful discussions concerning the microfluidic chamber. We also thank Sabrina Gärtner and Maximilian Peters for contributing to the experiments.

■ REFERENCES

(1) Puurunen, R. L. *J. Appl. Phys.* **2005**, *97*, 121301−1.
(2) Knez, M.; Nielsch, K.; Niinistö, L. *Adv. Mater.* **2007**, *19*, 3425−3438.
(3) Jeong, D.; Lee, J.; Shin, H.; Lee, J.; Kim, J. *J. Korean Phys. Soc.* **2004**, *45*, 1249−1252.
(4) Detavernier, C.; Dendooven, J.; Sree, S. P.; Ludwig, K. F.; Martens, J. A. *Chem. Soc. Rev.* **2011**, *40*, 5242−5253.
(5) Martinson, A. B. F.; Elam, J. W.; Hupp, J. T.; Pellin, M. J. *Nano Lett.* **2007**, *7*, 2183−2187.
(6) Bachmann, J.; Jing, J.; Knez, M.; Barth, S.; Shen, H.; Mathur, S.; Gösele, U.; Nielsch, K. *J. Am. Chem. Soc.* **2007**, *129*, 9554−9555.
(7) Wu, Y.; Assaud, L.; Kryschi, C.; Capon, B.; Detavernier, C.; Santinaccic, L.; Bachmann, J. *J. Mater. Chem. A* **2015**, *3*, 5971−5981.
(8) Shevjakov, A. M.; Kuznetsova, G. N.; Aleskovskii, V. B. *Chemistry of High-Temperature Materials*; Proceedings of the Second USSR Conference on High-Temperature Chemistry of Oxides, Leningrad, USSR, November 26−29, 1965 Nauka, Leningrad, USSR, 1967; pp 149−155.
(9) Suntola, T.; Antson, J. U.S. Patent 4,058,430, November 15, 1977.
(10) Ariga, K.; Hill, J. P.; Ji, Q. *Phys. Chem. Chem. Phys.* **2007**, *9*, 2319−2340.
(11) Decher, G.; Hong, J. D.; Schmitt, J. *Thin Solid Films* **1992**, *210-211*, 831−835.
(12) Lvov, Y.; Decher, G.; Möhwald, H. *Langmuir* **1993**, *9*, 481−486.
(13) Li, J. J.; Wang, Y. A.; Guo, W.; Keay, J. C.; Mishima, T. D.; Johnson, M. B.; Peng, X. *J. Am. Chem. Soc.* **2003**, *125*, 12567−12575.
(14) Pathan, H. M.; Lokhande, C. D. *Bull. Mater. Sci.* **2004**, *27*, 85−111.
(15) Gregory, B. W.; Stickney, J. L. *J. Electroanal. Chem. Interfacial Electrochem.* **1991**, *300*, 543−561.
(16) Thambidurai, C.; Kim, Y.-G.; Stickney, J. L. *Electrochim. Acta* **2008**, *53*, 6157−6164.
(17) All experimental details are described in the Supporting Information.
(18) Aarik, J.; Aidla, A.; Uustare, T.; Ritala, M.; Leskela, M. *Appl. Surf. Sci.* **2000**, *161*, 385−395.
(19) Ritala, M.; Leskelä, M.; Niinistö, L.; Haussalo, P. *Chem. Mater.* **1993**, *5*, 1174−1181.
(20) Sinha, A.; Hess, D. W.; Henderson, C. L. *J. Vac. Sci. Technol. B* **2006**, *24*, 2523−2532.
(21) Leskela, M.; Ritala, M. *Thin Solid Films* **2002**, *409*, 138−146.
(22) George, S. M. *Chem. Rev.* **2010**, *110*, 111−131.
(23) Methaapanon, R.; Bent, S. F. *J. Phys. Chem. C* **2010**, *114*, 10498−10504.
(24) Gao, X.; Bare, S. R.; Fierro, J. L.G.; Banares, M. A.; Wachs, I. E. *J. Phys. Chem. B* **1998**, *102*, 5653−5666.
(25) Burton, B. B.; Goldstein, D. N.; George, S. M. *J. Phys. Chem. C* **2009**, *113*, 1939−1946.
(26) Vangelista, S.; Mantovan, R.; Lamperti, A.; Tallarida, G.; Kutrzeba-Kotowska, B.; Spiga, S.; Fanciulli, M. *J. Phys. D: Appl. Phys.* **2013**, *46*, 485304−485313.
(27) Bachmann, J. *Beilstein J. Nanotechnol.* **2014**, *5*, 245−248.
(28) Grünzel, T.; Lee, Y. J.; Kuepper, K.; Bachmann, J. *Beilstein J. Nanotechnol.* **2013**, *4*, 655−664.
(29) Bachmann, J.; Zierold, R.; Chong, Y. T.; Hauert, R.; Sturm, C.; Schmidt-Grund, R.; Rheinländer, B.; Grundmann, M.; Gösele, U.; Nielsch, K. *Angew. Chem., Int. Ed.* **2008**, *47*, 6177−6179.
(30) Klaus, J. W.; Sneh, O.; George, S. M. *Science* **1997**, *278*, 1934−1936.
(31) Klaus, J. W.; George, S. M. *Surf. Sci.* **2000**, *447*, 81−90.
(32) Zhan, G.-D.; Du, X.; King, D. M.; Hakim, L. F.; Liang, X.; McCormick, J. A.; Weimer, A. W. *J. Am. Ceram. Soc.* **2008**, *91*, 831−835.
(33) Green, J. M.; Dong, L. F.; Gutu, T.; Jiao, J.; Conley, J. F.; Ono, Y. *J. Appl. Phys.* **2006**, *99*, 094308.
(34) Brennan, T. P.; Ardalan, P.; Lee, H. B. R.; Bakke, J. R.; Ding, I. K.; McGehee, M. D.; Bent, S. F. *Adv. Energy Mater.* **2011**, *1*, 1169−1175.
(35) Rooth, M.; Quinlan, R. A.; Widenkvist, E.; Lu, J.; Grennberg, H.; Holloway, B. C.; Hårsta, A.; Jansson, U. *J. Cryst. Growth* **2009**, *311*, 373−377.
(36) Musić, S.; Filipović-Vinceković, N.; Sekovanić, L. *Braz. J. Chem. Eng.* **2011**, *28*, 89−94.
(37) Feifel, S. C.; Lisdat, F. *J. Nanobiotechnol.* **2011**, *9*, 59.
(38) Trukhin, A. N.; Fitting, H.-J.; Barfels, T.; von Czarnowski, A. *J. Non-Cryst. Solids* **1999**, *260*, 132−140.
(39) Burton, B. B.; Kang, S. W.; Rhee, S. W.; George, S. M. *J. Phys. Chem. C* **2009**, *113*, 8249−8257.
(40) McCafferty, E.; Wightman, J. P. *Surf. Interface Anal.* **1998**, *26*, 549−564.
(41) Alam, A. U.; Howlader, M. M. R.; Deen, M. J. *ECS J. Solid State Sci. Technol.* **2013**, *2*, 515−523.
(42) Hatano, M.; Ishihara, K. *Yuki Gosei Kagaku Kyokaishi* **2008**, *66*, 564−577.
(43) Klatt, T.; Markiewicz, J. T.; Sämann, C.; Knochel, P. *J. Org. Chem.* **2014**, *79*, 4253−4269.

DOI: 10.1021/acs.nanolett.5b01424
Nano Lett. 2015, 15, 6379−6385